A Simple In-Situ Sensor for Snow Grain Size Measurement

A. KASURAK,[1] R.E.J. KELLY,[1] J. KING[1]

ABSTRACT

Grain size (GS) is a standard parameter required for models that simulate the evolution of the microphysical state of a snowpack, energy and mass balance, or radiative transfer for remote sensing. Determining the size of a grain of snow is subjective and complex requiring skill to measure repeatably. A typical method is to measure the dimensions of sample snow grains on a grid under magnification. However, removal of grain clusters frequently breaks their structure apart, causing under-estimation. Subjectivity of measurement is introduced through the selection of which grains to measure; this introduces bias in the grain dimension statistics.

A new instrument is constructed from a snow density cutter that estimates snow grain size from transmission loss of light through a sample. Following the success of the prototype (green LED and photoresistor with a 0.67 R^2 to grain size), a second and third version were built and field tested in early 2012. The second version is a 5 × 5 × 5 cm ended box cutter with 2-axis measurement by paired photoresistors and phototransistors. Transmitting LEDs are blue, green, NIR, and white. The third version 4-cm transparent plastic jar with opposed blue LED and phototransistor. Data logging is managed with an Arduino unit. Conceptually, the devices operate identically to the first version: the difference in received light between the empty and with-snow states are compared to the parameters of the sample snow.

Linear regression results with the second sensor show equal performance to the first version; and after controlling for size, grain properties such as aggregation are significant. Together, the three prototype sensors and two years of data describe a low-cost functional system for fast retrieval of snow grain size without observer bias.

Keywords: Snow, snow grain size, instrument, snow density

INTRODUCTION

Grain size is an important standard parameter required for models that simulate the evolution of the microphysical state of a snowpack, energy and mass balance, or radiative transfer for remote sensing (Fierz et al., 2009; Lehning et al., 2002; Pomeroy et al., 1993; Pulliainen et al., 1999). Grain size contributes a significant control on snow albedo (Warren, 1982; Zhou et al., 2003a). Determining the size of a grain of snow is subjective and complex, requiring practice (Fierz et al., 2009). Typical measurements are visual estimations of one or two axes, under magnification. Grain size can be objectively measured by sterology, tomography, and macro photography. Other field measures of grain size have been developed to avoid the problems of subjective measurement such as optical diameter or specific surface area (SSA) (Domine et al., 2006; Grenfell and Warren, 1999; Mitchell, 2002; Painter et al., 2007), and correlation length (Mätzler, 2002). These techniques include such instruments as integrating sphere point measurements of near infra-red

[1] University of Waterloo. 200 University Avenue West, Waterloo, Ontario, Canada. N2L 3G1; akasurak@uwaterloo.ca.

(NIR) reflectance, NIR reflectance photography, grain microphotography, snow penetrometer (e.g., Langlois et al., 2010; Matzl and Schneebeli, 2006; Schneebeli et al., 1999). These measurements are also more directly relatable to those used in radiative transfer modeling.

Although the methods for determining grain size (D_{obs}) (GS) or SSA are relatively robust, they are either not rapid, requiring manual post-processing to determine the GS, or require expensive hardware. This combination of expertise and cost restricts applicability. The conventional method, hand measurement on a grain card, is time consuming in the field with many repeat observations required to determine the distribution of GSs in the sample. In these repeat measurements a subjective choice of which grains represent the sample must be made and a further subjective choice of the grain boundaries. In sintered or faceted grains, boundary distinction is very difficult.

Therefore there are three main problems in identifying snow GS.

1. Grains are not distinct and will join other grains. In constructive metamorphism, a new facet can grow from the side of an existing grain. Identifying the boundaries of a selected snow grain is highly subjective.
2. Grains form structures, such as vertical chains, that strongly influence the EM response of the snowpack while not being measured by hand techniques.
3. It is not clear what measurements should be taken to characterize the interaction of electromagnetic radiation with snow grains: one axis, two axis, SSA, diameter, volume, or another.

This study investigates the feasibility of using transmitted light to retrieve snow GS rather than the more common reflected light. Discrete wavelength bands across the visible spectrum are used rather than single NIR wavelengths. Visible light has greater penetration depth, and may be required for measurements of high density-low GS packs. The approach is most similar to the NIR reflectance technique but provides advantages in lower equipment cost and retrieval speed.

The study was conducted over two winters (2010–2011 and 2011–2012) with most samples taken from the sub-arctic tundra of Churchill, Manitoba (Figure 1). Three separate versions of the sampling instrument were built, the snow grain sensor (SGS)1–3, detailed in the *METHODS: Experiment 1: Proof of concept of the snow grain sensor* and the *METHODS: Experiment 2: Sampler design impacts* Sections. Sampling in 2010–2011 was done in late March, and depth hoar growth was more complete, as compared to the low accumulation and metamorphism of February 2012. Other samples were taken in Waterloo (2011, 2012) and Ottawa (2012), Ontario. The *Methods* and *Results* Sections describe five experiments ranging from simple analysis through sensor design sensitivity. Experiment one and five are most relevant to the operational estimation of GS.

METHODS

Recent studies have demonstrated the GS response to reflectance measurements in NIR. In this study we use in-situ of transmission loss rather than measurements of reflectance, as isolating the sample from external light reduces the complexity of parameter retrieval. The measure is also then a bulk properties measurement and will not be as affected by surface preparation, since any broken and compacted grains along the boundary of the volume are a small fraction of the path length. Zhou et al. (2003a) provide a recent discussion of visible and NIR interactions with a variety of snow types, demonstrating the theory which underlies this instrument. The critical extinction depth of light from 200 through 2800 nm described in a discrete ordinal radiative transfer (DISORT) simulated semi-infinite pack of variable density and GS. Higher density and smaller grain sizes were found to reduce the critical depth. If we invert the relationship for a fixed depth, less than the critical thickness, then the loss in light travelling through the snow will be proportional to the GS and depth (Nolin et al., 1993; Zhou et al., 2003a).

Five experiments with the device were conducted to assess the performance over a range of permutations of sensor design factors and operational parameters. In the *Experiment 1: Proof of*

concept of the snow grain sensor Section, the basic principle of operation is demonstrated with SGS-1, the simplest configuration. This is then expanded in the *Experiment 2: Sampler design impacts* Section with a larger snow sample size and different sensor electronics in SGS-2 and SGS-3. The *Experiment 3: Sensitivity to wavelength* Section considers the performance of the expanded range wavelengths offered by SGS-2 and 3. The *Experiment 4: Sensitivity to orientation* and *Experiment 5: On grain shape* Sections examine the effects of rotating the sensor by 90 degrees and of the effects of grain shape, respectively. The *Experiment 5: On grain shape* Section also revisits the operational retrieval of the *Experiment 1: Proof of concept of the snow grain sensor* Section with the information from all experiments to produce a final method.

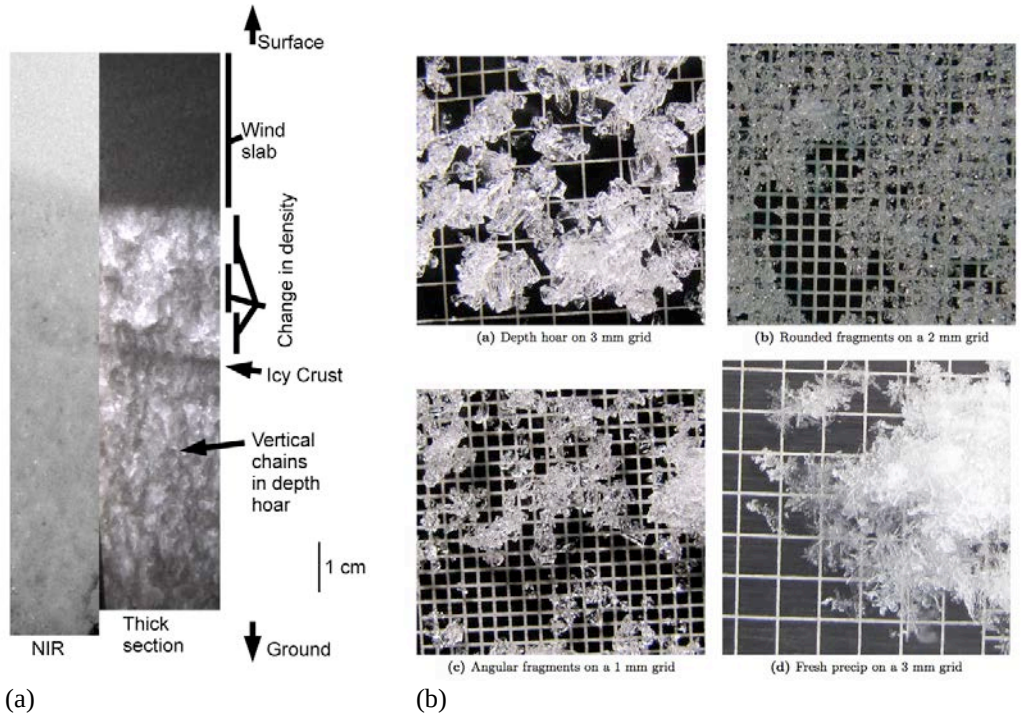

Figure 1. (a) Depth hoar chains in tundra snow and (b) samples of grain classification.

Experiment 1: Proof of concept of the snow grain sensor

The SGS-1 was constructed as the minimal possible system to examine the transmissivity (T_r) of light through a contained snow sample. It consisted of a 50 cm^3 box snow density cutter with a pair of internal prongs 1.5 cm containing the transmitting LED at 530 nm (green, diffuse) and receiving photodetector with matched spectral sensitivity, a 50 k ohm (Figure 2c). Readings of received light at the photodetector, as a measure of transmission, were taken directly with a multimeter. Green light was chosen as it has been shown to have a high penetration in a wide range of snowpacks (Zhou et al., 2003a). In operation, the cutter is inserted into the snowpack, weighed, then a covering is added to completely remove ambient light. The filled resistance (Figure 2) is measured, along with ambient temperature. After the sample is discarded, the instrument is again covered; and an empty resistance is measured. This background measurement is then subtracted to provide a measure of the loss in transmission through the pack.

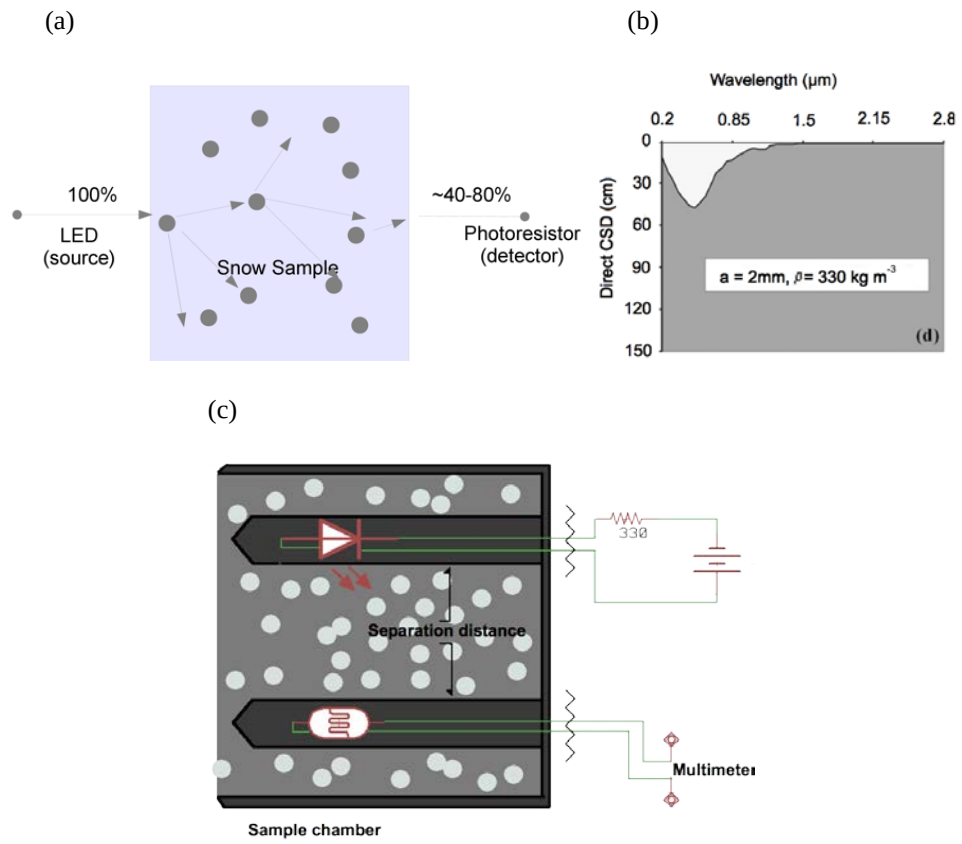

Figure 2. (a) Function of the GS probe. (b) Zhou et al. (2003a), Figure 2(d), relationship between extinction depth, wavelength, grain size, and density for natural light. (c) Schematic diagram of SGS-1 components. Measurement of resistance is taken via multimeter across pins 1 and 2.

For validation, hand measurements of grain size were taken on a ruled card under 10x magnification. Nine grains for each sample were measured for long and short axis. All measurements were taken by the same observer to eliminate inter-observer bias. Snow and air temperature were recorded; and in 2011–2012, macro photographs of the grain sample were taken. Snow density was measured in 2010–2011 using a standard 100 cm^3 for reference as the SGS-1 had a small volume and produced unreliable density estimates. In 2011–2012, density was measured directly using the 125 cm^3 SGS-2.

Overall, 21 samples were made in 2010–2011, with relevant properties of the snow and sensors summarized in Table 1, with associated number of measurements. For this experiment, the long and short axis measurements of grain size were averaged (mean) together to create one composite value.

Table 1. Summary of characteristics of the samples and instruments.

Parameter	2010–2011		2011–2012	
Samples	21		73	
Orientation (H, V)[1]	7, 9		30, 29	
Parameter	Min	Max	Min	Max
Density (g cm^3)	0.11	0.37	0.14	0.49
Temperature (°C)	-20	0	-25	-1.2
Mean GS (mm)	0.26	2.18	0.25	4.77
Wavelength	Green	Green	Blue	NIR

[1] Number of samples in each orientation: horizontal, vertical.

To describe a relationship between observed loss in transmission and hand measured grain size with a limited data set, the principle regressors described by Zhou et al., GS and density were considered first and independently. With correlation between density and GS combined with a small data set, regression coefficient estimation will be unstable and is better avoided. Therefore, only two models were tested: $T_n \sim D_{obs}$, and $T_n \sim D_{obs} + \rho_{snow}$. Furthermore, the non-linear form of the $T_n \sim D_{obs}$, relationship was linearlized using the effective grain size formula from the Helsinki University of Technology radiative transfer (HUT) model: $D^*_{obs} = 1.5 \bullet e^{(-1.5 \bullet D_{obs})}$ (Kontu and Pulliainen, 2010).

Experiment 2: Sampler design impacts

Two additional grain sensors were built. The first of these, SGS-2 (Figure 3), had a larger box cutter, 5×5×5 cm, with horizontal transmission (via independent LEDs centered and flush with the inside face of the cutter) in green, blue, and NIR and vertical transmission in green, blue, NIR, and white. Reception was done with V and H paired photodetectors, a visible–NIR sensitive phototransistor (P_T), and a visible sensitive photoresistor (P_R). Phototransistors were used to test the utility of a faster response time than P_R. The second new instrument, SGS-3, had one blue transmitter and opposed P_T; the sample is made using a separate clear plastic tube which is then placed in the transmission chamber and may be rotated to sample V and H relative to original snowpack orientation. Sample tube outer diameter, and therefore sensor separation, was 4.0 cm.

Figure 3. SGS-2 prototype instrument.

Raw T_r measurements differed by SGS version and receiver. SGS-1 measured resistance across the photoresistor using a hand held multimeter. SGS-2 and 3 use an off-the-shelf microcontroller (Arduino) as a datalogger and read voltage rather than resistance. To normalize T_r and allow comparison between bands and between sensors, the maximum observed T_r for each band was set to 1.0; and all readings in that band scaled to it. Ideally, absolute calibration of transmitter and receiver would allow for specific loss in radiance to be used.

The addition of numerous modes of transmission and reception necessitates a naming scheme; therefore, these combinations are referred to as "bands", and denoted $B_{transmitter \rightarrow reciever}$, each specified with an orientation, horizontal (H) or vertical (V), and class. For transmitters, the class is the spectrum of light emitted by the LED—green (G), blue (B), white (W), or NIR (I)—while the receiver is a photoresistor (denoted "O" for primarily visible [optical] sensitivity) or phototransistor ("I," for higher NIR sensitivity). For example, the combination of a horizontal green LED transmitting to a horizontal photoresistor would be labeled $B_{HG \rightarrow HO}$.

Data from SGS-1 was directly comparable with $B_{HG \rightarrow VI}$ of SGS-2 and $B_{*B \rightarrow VI}$ with SGS-3. This data was compared to examine the difference in sampler geometry. A regression between measured T_r and GS was performed as in the *Experiment 1: Proof of concept of the snow grain sensor* Section, after normalizing the measured value (hereafter, normalized transmissivity [T_n]).

Experiment 3: Sensitivity to wavelength

SGS-2 can be used to examine the wavelength dependency of the attenuation-GS relationship. Four different wavelengths of light were included, red, green, blue, NIR, along with white, a composite (see Table 2). Shorter wavelengths will undergo increased scattering, while longer wavelengths are better absorbed (Dozier et al., 2009).

Table 2. Properties of the transmitters and receivers.

LED color	Peak wavelength (nm)	Intensity[1]
Green	540	80
Blue	470	1500
White	450, 550[2]	2000
NIR	940	3.6
Receiver	peak wavelength (nm)	
Photoresistor (P_R)	520	
Phototransistor (P_T)	940	

[1] Intensity in milli-candela (mcd) for visible spectrum and $mW \bullet Sr^{-1}$ NIR and ultra-violet (UV).

[2] White LED light produced by phosphor stimulation from blue light, giving a narrow peak at 450 nm and a wide half-power peak at 550 nm.

The various combinations of transmission and reception were measured for SGS-2 observations in 2011–2012. Plots of transmission against adjusted mean GS (D^*_{obs}, *Experiment 1: Proof of concept of the snow grain sensor* Section) were used to evaluate the relative sensitivity of the different bands at a variety of GS. From the work by Zhou et al. (2003a), who modeled critical extinction depth using radiative transfer equations solved with DISORT (Stamnes et al., 1988) and GOMsphere (Zhou et al., 2003b), we expect maximum penetration and, therefore, minimum attenuation at approximately 500 nm (blue).

Experiment 4: Sensitivity to orientation

Some snow packs may develop multi-grain structures with preferred orientation, such as depth hoar chains (Figure 1) Pfeffer (2002). Additional features, including grain size gradients, layer boundaries, and crusts, will create anisotropy in the sample. To determine if there is a difference in the horizontal and vertical T_n and what might explain it, a procedure to sample the same layer twice orthogonally was adapted. SGS-1 was rotated 90 degrees and a second sample was taken. SGS-2 had both horizontal and vertical bands (referred to as "paired" bands or sensors), and was also rotated as SGS-1. SGS-3 samples, collected in a clear plastic sample vial, are rotated in the sample chamber to measure transmission through and along the in-situ plane.

Two potential sources for a difference in orthogonal measurements are (1) non-random orientation of elongated grains, e.g., hoar chains, providing columnar voids in the snowpack; and (2) non-uniform distribution of grains, for instance a vertical gradient of GS or ρ_{snow} or an ice lens sampled between the vertical components, but not the horizontal. The experiment was conducted on uniform windslab, uniform depth hoar, across a layer boundary of windslab and depth hoar, and across an icy crust in depth hoar.

Experiment 5: On grain shape

Grain shape is expected to influence the propagation of energy through the pack, as shape defines the relationship between geometric observed size and effective diameter, described by Kokhanovsky and Zege (2004), Mätzler (1997), and Mitchell (2002). This relationship was observed by Langlois et al. (2010), who model D_{opt} (after Kokhanovsky and Zege [2004]) from NIR reflectance and observe that at larger GS shape informs the relationship. However they were unable to develop a useful relationship.

Table 3. Summary of grain properties by class.

Grain type	D_{obs}	stdev (D_{obs})	sphericity	density	n
Angular	0.80	0.53	0.79	0.35	36
Fragments	0.85	0.56	0.80	0.34	42
Clusters	0.98	0.71	0.80	0.37	21
Rounded	1.01	0.65	0.87	0.33	10
Depth hoar	1.80	0.93	0.82	0.29	21
Fresh Precip.	2.05	2.12	0.73	0.12	6

We first look for confounders in measuring the shape effect, namely grain size and density, then use regression to assess the explanatory power of shape. The effect of the confounding variables was estimated through the regression relationship developed in the *Experiment 1: Proof of concept of the snow grain sensor* Section, the residuals of which represent the portion of the measured attenuation that is not described by grain size and density. Table 3 describes the available samples by their grain class. Each snow sample was given descriptors of its grains by visual inspection under 10x magnification with a hand lens. These attributes were rounded (R), angular (A), fragmented (F), depth hoar (D) (both cups and facets), clustered (C) (depth hoar chains, melt-freeze clusters, inter grown crystal aggregates), and intact precipitation forms (P). Each grain's sphericity was also measured as the ratio of long to short axis measurements; all 9 sphericity measurements for a sample were then averaged. A sample of each grain class is presented in Figure 1b.

RESULTS

Experiment 1: Proof of concept of the snow grain sensor

A regression was produced in the form: $T_n \sim D_{obs}$, with the transformations to linearize the relationship as in the *Experiment 1: Proof of concept of the snow grain sensor* Section on the SGS-1 data alone. The regression has a significant adjusted R^2 (R^2_{adj}) of 0.72, a mean absolute error (MAE) of 0.13 mm, and negligible bias. The model intercept is 0.042, and the coefficient for GS is 0.60. Further adding density to the relationship explained very little of the observed change in resistance (as a measure of T_n) and was no longer statistically significant. The data are shown in Figure 4 with the resultant regression line plotted.

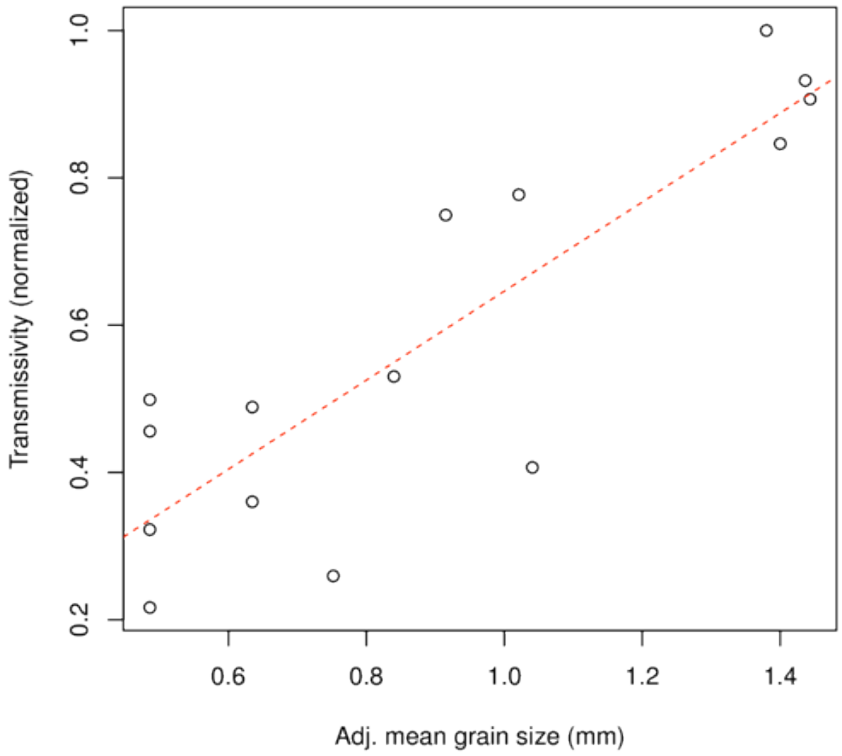

Figure 4. Calibration regression of optical loss in transmission to grain size.

Experiment 2: Sampler design impacts

Two groups of bands are directly comparable: SGS-1 green with $B_{HG \rightarrow VO}$ and $B_{VG \rightarrow V*}$ and $B_{*B \rightarrow VI}$ compared to SGS-3 (Figure 5). Overall, the separation distance and wavelength of SGS-2, green, diagonal (horizontal transmit to vertical receive) seems most favorable in capturing GS, demonstrating a linear relationship in the T_n. GS plot. No samples taken with SGS-1 were measured which attenuated almost all of the light; although this may indicate potential for sampling of smaller, higher density grains rather than a failure to tune instrument sensitivity. The larger separation distance of $B_{VG \rightarrow V*}$ SGS-2, shows a strong spread (heteroscedasticity) with large GS; although this may be explained as the final points above a D^*_{obs} of 1.4 mm are a wide range of grain shapes: fresh stellar dendrites, depth hoar, rounded melt clusters, and fragmented hoar. The effect of varying grain shapes is explored in the *Experiment 4: Sensitivity to orientation* and *Experiment 5: On grain shape* Sections.

The calibration regression is revisited in experiment 5 for a combined SGS-1, 2 dataset. This combined set has more observations, allowing for additional regression analysis.

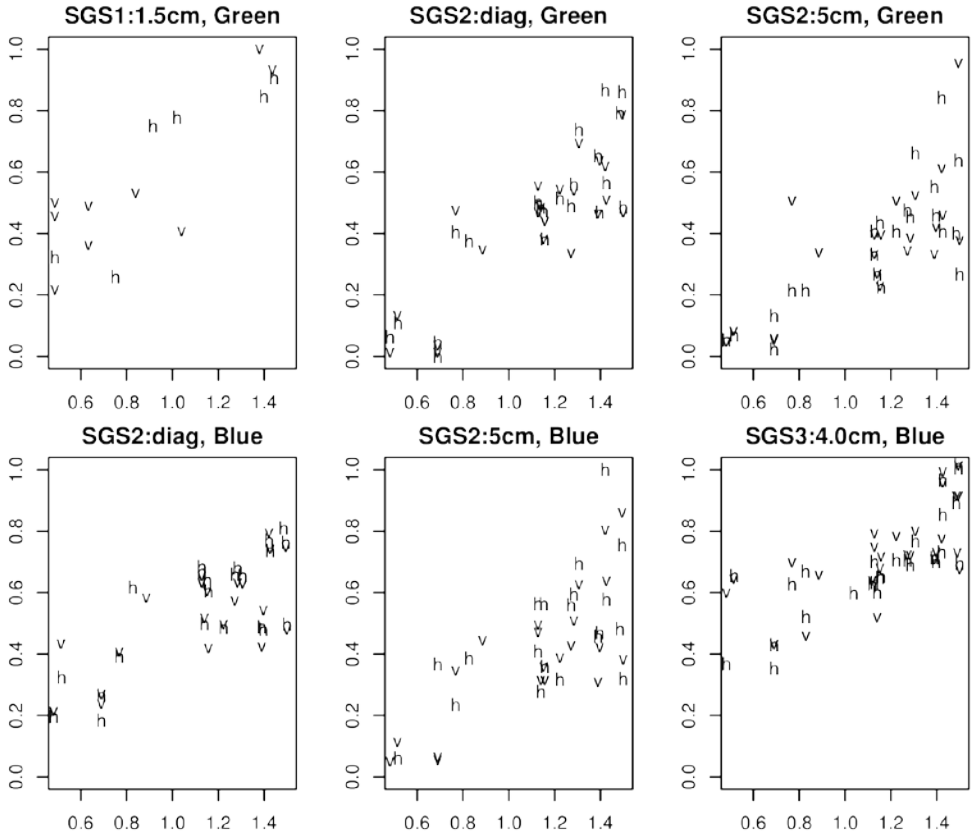

Figure 5. Normalized transmissivity, T_n vs. D^*_{obs} vs. by separation for top row: SGS-1 (green), SGS-2 $B_{HG \rightarrow VO}$, SGS-2 $B_{VG \rightarrow V*}$; bottom row: SGS-2 $B_{HB \rightarrow VI}$, SGS-2 $B_{VB \rightarrow VI}$, SGS-3 (blue). h: horizontal sensor orientation, v: vertical sensor orientation.

Experiment 3: Sensitivity to wavelength

Independent regressions of $T_n \sim D^*_{obs}$ for each band (presented in Table 6, for those with $R^2_{adj} > 0.5$) describe the wavelength response of the sensor. Three bands are shown in Figure 6. Notably, green bands are systematically lower in SGS-2, allowing for a merger of the data by adding 0.23 (the magnitude of the regression term specifying sensor in $T_n \sim D^*_{obs} + \rho_{snow} +$ sensor, for the joint dataset, presented in the *Experiment 5: On grain shape* Sections) to T_n.

Three problems in the data were common to the excluded relationships:

1. T_n all very close to 1.0, the different samples did not attenuate sufficient light to bring the receptor into the linear response range, and it remained saturated.
2. Insufficient light penetrated the sample to bring the sensor into the linear response range, all readings close to 0.
3. Little to no variability between samples in T_n, band is not responsive to GS.

Those bands that did produce a result were linear to exponential in response to GS. The similarity in response between the P_T P_R is evident in the nearness of the R^2_{adj} models (e.g., $B_{VW \rightarrow VI}$ and $B_{VW \rightarrow VO}$). This indicates that the illumination duration was sufficient to saturate the P_R and that the P_T was able to capture the same information. This is not always the case, as with $B_{HG \rightarrow HO}$ and $B_{HG \rightarrow HI}$, wherein the lower illumination from the LED was seemingly insufficient to gain a response from the P_R. Overall, paired horizontal ($B_{H* \rightarrow H*}$) and vertical ($B_{V* \rightarrow V*}$) elements

performed better than diagonal arrangements (e.g., $B_{H^* \rightarrow V^*}$). Wavelengths were most responsive where transmission was expected to be maximized.

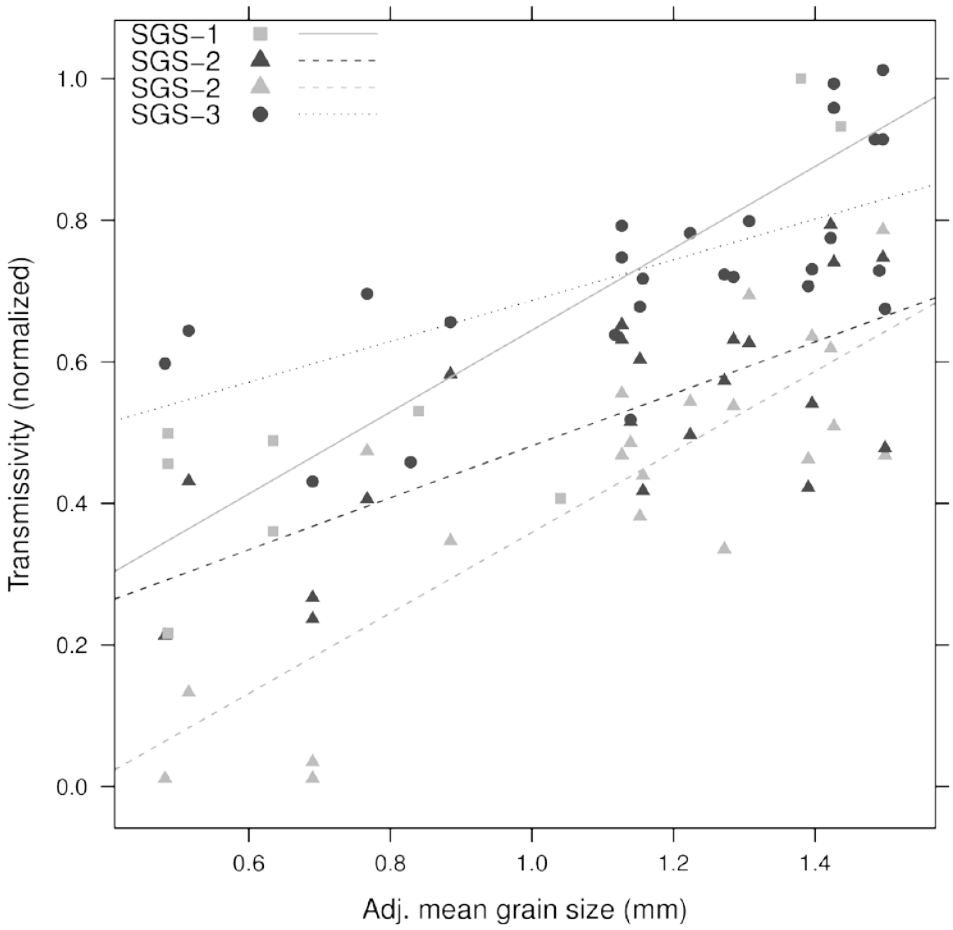

Figure 6. Grain size vs. attenuation for SGS-1, 2 (selected modes), 3. Symbol color indicates transmitting LED (light grey: green LED, dark grey: blue LED) . Lines show best fit of $T_n \sim D^*_{obs}$ per sensor and band.

Table 6. Results of the per band regressions ($Tn \sim D^*_{obs}$). All bands which did not meet $R^2_{adj} > 0.5$ are not shown.

Transmitter	Receiver[1]	Band label	R^2_{adj}	n
V (blue)	V (P_R)	$B_{VB \rightarrow VO}$	0.50	41
H (blue)	V (P_T)	$B_{VB \rightarrow VI}$	0.55	43
H (blue)	V (P_R)	$B_{VB \rightarrow HO}$	0.55	43
H (NIR)	V (P_T)	$B_{HI \rightarrow VI}$	0.56	43
V (green)	V (P_T)	$B_{VG \rightarrow VI}$	0.56	43
H (blue)	H (P_T)[2]	$B_{HB \rightarrow HI}$	0.62	27
V (white)	V (P_T)	$B_{VW \rightarrow VI}$	0.62	42
V (white)	V (P_R)	$B_{VW \rightarrow VO}$	0.64	43
H (green)	V (P_T)	$B_{HG \rightarrow VI}$	0.72	43
H (green)	H (P_R)[3]	$B_{HG \rightarrow HO}$	0.72	15

[1] Reception can be via photoresistor (PR), or phototransistor (PT, NIR sensitive).
[2] SGS-3.
[3] SGS-1, all others SGS-2.

Experiment 4: Sensitivity to orientation

The impact of taking a reading parallel to the layering (horizontal) or perpendicular to it (vertical) was tested in this experiment (physically performed either with $B_{HG \rightarrow HI}$ paired with $B_{VG \rightarrow VI}$ in SGS-2 [a "paired replicate"], or $B_{HG \rightarrow HI}$ taken twice with 90º of the sensor [a "rotational replicate"]); SGS-3 always takes rotational replicates, but of the same sample, while SGS-1 must resample. A measure, VH_{diff}, the difference in readings of the same sensor when rotated was calculated, for example, the VH_{diff} for $B_{HG \rightarrow HI}$ is calculated as $B_{HG \rightarrow HI}$ minus the rotated replicate $B_{HG \rightarrow HI}$. Paired replicates (only rotated replicates) were not used as differences in component values prevented direct comparison of bands through the introduction of an uncontrolled error term. An absolute calibration of the instrument should allow for these comparisons to be made. The results are presented in Table 7.

Table 7. Difference of T_n for different grain types, $B_{HG \rightarrow VI}$.

Grain Type	T_n	D^*_{obs}	VH_{diff} [1]	n	Wilcox[2]
Angular	0.42	1.11	0.01	11	0.30
Fresh Precip.	0.49	1.50	0.02	1	0.82
Fragments	0.45	1.10	0.02	13	0.30
Depth Hoar	0.55	1.25	0.03	8	0.74
Clusters	0.45	1.05	0.07	8	0.28
Rounded	0.52	0.99	0.07	4	0.70
All	0.51	1.18	0.03	17	–

[1] Reading with sensor oriented in V, minus reading of same snow layer with sensor rotated 90º to H.
[2] Wilcox rank sum test for difference of means

We see that clustered or chained grains have a seemingly different T_n; however, the Wilcoxon rank sum test indicates the difference is not significant. This lack of significance is likely due to the very small sample sizes. If we consider the VH_{diff} of all bands that score at least an R^2_{adj} 0.5, we find the clustered grain VH_{diff} to be 0.03, which is significantly different from the all grain value of 0.01. However, this test of significance does not properly account for the loss of information from the correlation between bands. Nevertheless, it remains suggestive of the idea that preferential grain structures give measurably different attenuation along and across their orientation.

The results from using SGS-1, which are also a small dataset, show qualitative differences between the horizontal and vertical orientation particularly around a thin ice layer embedded in depth hoar, as well as through horizontal and parallel (vertical) to the depth hoar chain structure.

These measurements indicate that it may be possible to retrieve a measure of structure by comparing the H and V observations taken from within a single layer.

Experiment 5: On grain shape

To explore the effects of grain shape on T_n, we must first remove the size dependence. This was done by linear regression on $T_n \sim D^*_{obs} + \rho_{snow}$ + sensor over SGS-1 and horizontal transmitting green, vertical IR receiving band ($B_{HG \rightarrow VI}$) of SGS-2. The sensor offset was found to be 0.23. This relationship has a statistically significant R^2_{adj} of 0.75. The formula, $T_n \sim D^*_{obs} + \rho_{snow}$ is that of the *Experiment 1: Proof of concept of the snow grain sensor* Section, with both density and GS included, as more observations are available, and the coefficients are comparable (intercept: 0.039, slope of GS: 0.55, ρ_{snow}: −0.40).

The residuals of this regression are then compared with the grain classification through regression, terms selected by bi-directional stepwise regression using BIC as the penalty criterion, producing residuals($T_n \sim D^*_{obs} + \rho_{snow}$ + sensor) ~ sphericity + sphericity^2 + is.rounded + is.precip. The rounded (slope: 0.11) and precipitation (slope: −0.097) classes were found to be significant, along with mean sphericity (slope: 3.7s −2.5s^2) when considered as a second order polynomial. This relationship between the residuals of the GS regression and the grain shape descriptors has an R^2_{adj} of 0.53. Multicolinearity was not an issue between selected grain descriptors.

We have demonstrated now that GS can be determined (within the limits of an empirical regression experiment) as a function of T_n, and that a significant portion of the unexplained variance of this function can be related to grain shape.

DISCUSSION

The calibration equations developed in experiment 1 and 5 demonstrate the validity of the theoretical relationship of Zhou et al. (2003a) between grain size (GS), density, and extinction over a wide variety of grain types and sizes, in both sub-arctic and maritime snow. The optical elements used are low-cost and operate over the visible and NIR wavelengths, which will limit the sensor's usefulness in soot or dust contaminated snowpacks. Longer wavelength NIR elements are possible but would increase the cost of the sensor.

The sensor is able to retrieve GS during the process of sampling density. The large size of the cutter reduces the resolution of the GS estimate, compared with extremely high resolution techniques such as NIR photography (Langlois et al., 2010).

The most similar published technique, the estimation of density via transmission by Gergely et al. (2010), demonstrated a slightly lower resolution than was found in this study and was used to estimate the more easily sampled physical quantity. It would be interesting to perform the above experiments with the integrating sphere setup to assess the loss in accuracy and precision from off-the-shelf components.

Figure 2 in Domine et al. (2006), relating the correlation of SSA to reflectance by wavelength, bears further investigation with a minima near zero at 600 nm as D_{obs} relatable to D_{opt} thus SSA and the correlation of GS by transmission is strong at these wavelengths.

Future work on the instrument will resolve the lost bands by dynamically adjusting the transmission strength to avoid saturating the receivers. Additional sample collection will allow full exploration of grain shape and sensor orientation. Extension of the observed wavelengths to 405 nm is underway.

CONCLUSION

A sensor has been described that rapidly measures snow GS with an unbiased observation of loss in transmission of green light in experiment 1. This sensor was expanded in experiment 2 and 3 to cover additional wavelengths, physical dimensions, and optical elements. Additionally, within the constraints of the available field data for calibration and validation, orientation and grain shape-dependent electromagnetic properties of the snow pack were observed. These measurements are user-independent and thus transferable between research teams and through a succession of researchers on one project. The low cost, rapidity, and ease of use of the sensor removes any barriers to its wider use.

In contrast to hand and photographic techniques, the sensor uses the same properties of the snow that are of interest to remote-sensing snow modelers. Calibration to measure SSA would likely be possible but cannot be done without a validation dataset.

Total sensor cost was under one dollar for SGS-1, not including a multimeter or analog to digital converter to read the output. SGS-2, 3 cost approximately $50 including the data logger and density cutter.

ACKNOWLEDGEMENTS

This experiment was funded through an NSERC discovery grant to R. Kelly and through the Northern Scientific Training Program. Special thanks to Josh King for in-field technical expertise and spare parts and to the Phillips family expedition. Thanks to Nicole Kasurak for allowing two cubic feet of snow to remain in the family freezer for two years.

REFERENCES

Domine F, Salvatori R, Legagneux L, Salzano R, Fily M, Casacchia R. 2006. Correlation between the specific surface area and the short wave infrared (swir) reflectance of snow. *Cold Regions Science and Technology* **46**(1): 60–68.

Dozier J, Green RO, Nolin AW, Painter TH. 2009. Interpretation of snow properties from imaging spectrometry. *Remote Sensing of Environment* **113**(Supplement 1): S25–S37. ISSN 0034-4257, 10.1016/j.rse.2007.07.029, Imaging Spectroscopy Special Issue.

Fierz C, Armstrong R, Durand Y, Etchevers P, Greene E, McClung DM, Nishimura K, Satyawali PK, Sokratov SA. 2009. *The International Classification for Seasonal Snow on the Ground*. IHP-VII Technical Documents in Hydrology No. 83, IACS Contribution No. 1. International Association of Cryospheric Sciences. UNESCO: Paris, France.

Gergely M, Schneebeli M, Roth K. 2010. First experiments to determine snow density from diffuse near-infrared transmittance. *Cold Regions Science and Technology* **64**(2): 81–86. ISSN 0165-232X, DOI: 10.1016/j.coldregions.2010.06.005, international Snow Science Workshop 2009 Davos.

Grenfell T, Warren S. 1999. Representation of a nonspherical ice particle by a collection of independent spheres for scattering and absorption of radiation. *Journal of Geophysical Research* **104**(D24): 31697–31709. 10.1029/1999JD900496.

Kokhanovsky AA, Zege EP. 2004. Scattering optics of snow. *Applied Optics* **43**(7): 1589–1602. 10.1364/AO.43.001589.

Kontu A, Pulliainen J. 2010. Simulation of spaceborne microwave radiometer measurements of snow cover using in situ data and brightness temperature modeling. *Geoscience and Remote Sensing, IEEE Transactions on* **48**(3): 1031–1044. ISSN 0196-2892, 10.1109/TGRS.2009.2030499.

Langlois A, Royer A, Montpetit B, Picard G, Brucker L, Arnaud L, Harvey-Collard P, Fily M, Goïta K. 2010. On the relationship between snow grain morphology and in-situ near infrared calibrated reflectance photographs. *Cold Regions Science and Technology* **61**(1): 34–42. ISSN 0165232X, 10.1016/j.coldregions.2010.01.004.

Lehning M, Bartelt P, Brown B, Fierz C, Satyawali P. 2002. A physical SNOWPACK model for the Swiss avalanche warning Part II. Snow microstructure. *Cold Regions Science and Technology* **35**(3): 147–167. ISSN 0165232X, 10.1016/S0165-232X(02)00073-3.

Matzl M, Schneebeli M. 2006. Measuring specific surface area of snow by near-infrared photography. *Journal of Glaciology* **52**(179): 558–564.

Mätzler C. 1997. Autocorrelation functions of granular media with free arrangement of spheres, spherical shells or ellipsoids. *Journal of Applied Physics* **81**: 1509.

Mätzler C. 2002. Relation between grain-size and correlation length of snow. *Journal of Glaciology* **48**(162): 461–466. 10.3189/172756502781831287.

Mitchell D. 2002. Effective diameter in radiation transfer: General definition, applications, and limitations. *Journal of the Atmospheric Sciences* **59**(15): 2330–2346. ISSN 1520-0469, 10.1175/1520-0469(2002)059<2330:EDIRTG>2.0.CO;2.

Nolin A, Shi J, Dozier J. 1993. Characterization of snow grain size in the near-infrared and microwave wavelengths. *Topical Symposium on Combined Optical-Microwave Earth and Atmosphere Sensing, Albuquerque, NM*, 51–54. Institute of Electrical and Electronics Engineers, Inc., 10.1109/COMEAS.1993.700179.

Painter T, Molotch N, Cassidy M, Flanner M, Steffen K. 2007. Instruments and methods: Contact spectroscopy for determination of stratigraphy of snow optical grain size. *Journal of Glaciology* **53**(180): 121–127. 10.3189/172756507781833947.

Pfeffer MR WT. 2002. Temperature gradient and initial snow density as controlling factors in the formation and structure of hard depth hoar. *Journal of Glaciology* **48**(163): 485–494. ISSN 00221430, 10.3189/172756502781831098.

Pomeroy JW, Gray DM, Landine PG. 1993. The prairie blowing snow model: Characteristics, validation, operation. *Journal of Hydrology* **144**(1–4): 165–192. ISSN 0022-1694.

Pulliainen J, Grandell J, Hallikainen M. 1999. HUT snow emission model and its applicability to snow water equivalent retrieval. *IEEE Transactions on Geoscience and Remote Sensing* **37**(3 Part 1): 1378–1390.

Schneebeli M, Pielmeier C, Johnson J. 1999. Measuring snow microstructure and hardness using a high resolution penetrometer. *Cold Regions Science and Technology* **30**(1-3): 101–114. 10.1016/S0165-232X(99)00030-0.

Stamnes K, Tsay SC, Wiscombe W, Jayaweera K. 1988. Numerically stable algorithm for discrete-ordinate-method radiative transfer in multiple scattering and emitting layered media. *Applied Optics* **27**(12): 2502–2509. doi:10.1364/AO.27.002502.

Warren SG. 1982. Optical properties of snow. *Reviews of Geophysics and Space Physics* **20**(1): 67–89.

Zhou X, Li S, Stamnes K. 2003a. Effects of vertical inhomogeneity on snow spectral albedo and its implication for optical remote sensing of snow. *Journal of Geophysical Research* **108**(D23): 4738. ISSN 0148-0227, 10.1029/2003JD003859.

Zhou X, Li S, Stamnes K. 2003b. *Gomsphere: A Comprehensive Geometrical Optics FORTRAN Code for Computation of Absorption and Single Scattering Properties of Large Dielectric Spheres—Documentation of Algorithm.* Technical report.